Spin-Orbit Fluctuations in Frustrated Heavy-Fermion Metal LiV_2O_4

K. Tomiyasu,[1,*] K. Iwasa,[1] H. Ueda,[2] S. Niitaka,[3] H. Takagi,[4] S. Ohira-Kawamura,[5] T. Kikuchi,[5] Y. Inamura,[5] K. Nakajima,[5] and K. Yamada[6]

[1]*Department of Physics, Tohoku University, Aoba, Sendai 980-8578, Japan*
[2]*Department of Chemistry, Kyoto University, Kyoto 606-8502, Japan*
[3]*RIKEN, 2-1 Hirosawa, Wako, Saitama 351-0198, Japan*
[4]*Department of Physics, University of Tokyo, Hongo 113-0033, Japan*
[5]*J-PARC Center, Japan Atomic Energy Agency, Tokai, Ibaraki 319-1106, Japan*
[6]*Institute of Materials Structure Science, High Energy Accelerator Research Organization, Oho, Tsukuba 305-0801, Japan*

(Received 26 May 2014; published 4 December 2014)

Spin fluctuations were studied over a wide momentum ($\hbar Q$) and energy (E) space in the frustrated d-electron heavy-fermion metal LiV_2O_4 by time-of-flight inelastic neutron scattering. We observed the overall $Q-E$ evolutions near the characteristic $Q=0.6$ Å^{-1} peak and found another weak broad magnetic peak around 2.4 Å^{-1}. The data are described by a simple response function, a partially delocalized magnetic form factor, and antiferromagnetic short-range spatial correlations, indicating that heavy-fermion formation is attributable to spin-orbit fluctuations with orbital hybridization.

DOI: 10.1103/PhysRevLett.113.236402 PACS numbers: 71.27.+a, 75.25.−j, 75.40.Gb, 78.70.Nx

The many-body problem is central to modern condensed-matter physics; i.e., how does one describe a large number of intricately interacting particles in solids and liquids? The concept of quasiparticles constitutes the basis of this problem; a system can be successfully treated as a collection of independent quasiparticles [1]. Examples include heavy fermions (HF) in metals and Cooper pairs in superconductors, in which conduction electrons are coupled with spins and lattices.

In 1997, the heaviest fermion system among d-electron systems, the metallic spinel LiV_2O_4 (nominally $V^{3.5+}$, $3d^{1.5}$), was discovered [2]. The ratio of the heat capacity to temperature C/T steeply increases with a large Sommerfeld coefficient $\gamma \simeq 400$ mJ mol^{-1} K^{-2} below the characteristic temperature $T^* \simeq 20$ K [3–5]. This followed the report of another d-electron HF system, $Y(Sc)Mn_2$, with $\gamma \simeq 140$ mJ mol^{-1} K^{-2} [6]. In both d-electron systems, the magnetic atoms form a geometrically frustrated pyrochlore lattice, suggesting a close connection between the HF and frustration.

LiV_2O_4 exhibits a weak cusp in magnetic susceptibility at T^* but no magnetic order at any measured temperature, indicating strong frustration [3]. Instead, powder inelastic neutron scattering (INS), nuclear magnetic resonance, and muon spin resonance (μSR) detect spin fluctuations below ~80 K down to 20 mK, which increase to antiferromagnetic (AF) short-range fluctuations described by $Q \simeq 0.6$ Å^{-1} below T^* [7–9], where the magnitude of the momentum $p=\hbar Q$. The 0.6-Å^{-1} nesting structure is also obtained by band calculations [10].

In addition, the electrical resistivity is metallic over the entire temperature range below room temperature and further decreases below T^* [3]. This decrease is different from the Kondo upturn, which is the fingerprint of conventional f-electron HF systems based on the Kondo coupling between the localized f-electron momenta and the conduction electrons. Further, the optical conductivity suggests that LiV_2O_4 changes from a poor metal to a coherent Fermi-liquid metal around T^* as the temperature decreases, as in the vicinity of a Mott insulator [11]. Photoemission also resulted in a resonance peak in the electronic density of states at ~4 meV above the Fermi level [12], which is also theoretically understood as the vicinity of the Mott insulator [13].

Thus, HF formation likely originates not from the conventional Kondo effect but from another novel electron correlation effect. The 0.6-Å^{-1} AF spin fluctuations driven by frustration will play a key role in HF formation. However, the overall correlations of the spin fluctuations in a wide (Q, E) space are still unclear, where E denotes the energy. For example, many Q-dependent characteristic frequencies were reported around 0.6 Å^{-1} [14], requiring a simple description by a response function. In contrast, no magnetic peak has been reported, other than the 0.6-Å^{-1} peak, hampering clarification of the spatial correlations. Different spatial-correlation models were also theoretically proposed, such as spin-orbit fluctuations with molecular V tetrahedra and one-dimensional (1D)-like chains [15,16].

In this study, we performed INS experiments on powder samples of LiV_2O_4 using a state-of-the-art time-of-flight spectrometer with large-solid-angle detectors, which allows us to investigate the spin fluctuations in a wide (Q, E) space. We used the direct geometry chopper spectrometer AMATERAS (BL14) at the Materials and Life Science

Experimental Facility (MLF) of the J-PARC spallation neutron source (Japan) [17]. The incident energy (E_i) was simultaneously set to 3.1, 4.7, 7.7, 15, and 24 meV using the multi-E_i technique, and the E resolution under elastic conditions was approximately 2.0%, 2.3%, 2.6%, 3.6%, and 4.5% to E_i, respectively. The main disk chopper speed was fixed at 300 Hz. The data were obtained by the UTSUSEMI software provided by the MLF [18]. Scattering from the empty-container background measurements was subtracted, and the absolute intensities were obtained by normalization to measure the incoherent scattering intensity from the sample. A powder sample of LiV_2O_4 was synthesized by a solid-state reaction method [19]. Li is in natural abundance. Approximately 7.3 g of the sample was placed onto an aluminum foil and shaped into a hollow cylinder with a thickness of 3 mm and a diameter of 20 mm in order to mitigate the neutron-absorption effects of Li nuclei as much as possible. The cylinder was kept in the thin aluminum container with He exchange gas that was placed under a cold head in a He closed-cycle refrigerator.

Results.—Figures 1(a) and 1(b) show the observed scattering intensity distributions in (Q, E) space. In the low-Q range below 1.5 Å^{-1}, which was previously reported [7,14], magnetic scattering is observed with fountainlike E evolution around 0.55 Å^{-1} at 6 K [Fig. 1(a)]. The scattering is paramagnetic around 0 Å^{-1} at 197 K [Fig. 1(b)]. The constant-E cross sections of the 6-K data are shown in Fig. 1(d). As E increases, the scattering broadens in Q.

In addition, we searched for another unreported magnetic signal in the high-Q range above 1.5 Å^{-1}. Figure 1(e) shows the cross sections at 2.5 meV. A broad and very weak peak appears between 2 and 3 Å^{-1} at 6 K. Further, the identical peak is observed with the different experimental conditions ($E_i = 15$ and 7.7 meV), indicating that this peak is not spurious but essential for the sample.

However, strong phonon scattering, consisting of the monotonically increasing component and the sharp peaks appearing only near strong Bragg reflections, is observed at 197 K, as shown in Fig. 1(e). Thus, to examine whether the 6-K broad peak is magnetic in origin, we correct the 197-K data with a Bose factor and subtract the corrected 197-K data [orange triangles] from the raw 6-K data [black squares] as the 6-K phonon component, as shown in the inset in Fig. 1(f). After this subtraction, the 2.4-Å^{-1} broad peak substantially remained [blue circles], indicating that another magnetic signal was found. We also remark that the sharp peaks are comparable between the raw data and the phonon component in intensity, as shown by the arrows, and cancel out each other in the magnetic component, supporting the validity of this subtraction procedure.

The wide-Q-range magnetic component combining the 0.6 and 2.4-Å^{-1} peaks are shown in Fig. 1(f). The low-Q phonons can be neglected compared to the 0.6-Å^{-1} strong magnetic peak in intensity. To smoothly connect the two peaks, however, we also subtracted the very weak low-Q phonon component, which was estimated by fitting and extrapolating the Bose-factor-corrected high-Q data except the sharp peaks with Q^2 and constant terms by the least-square method.

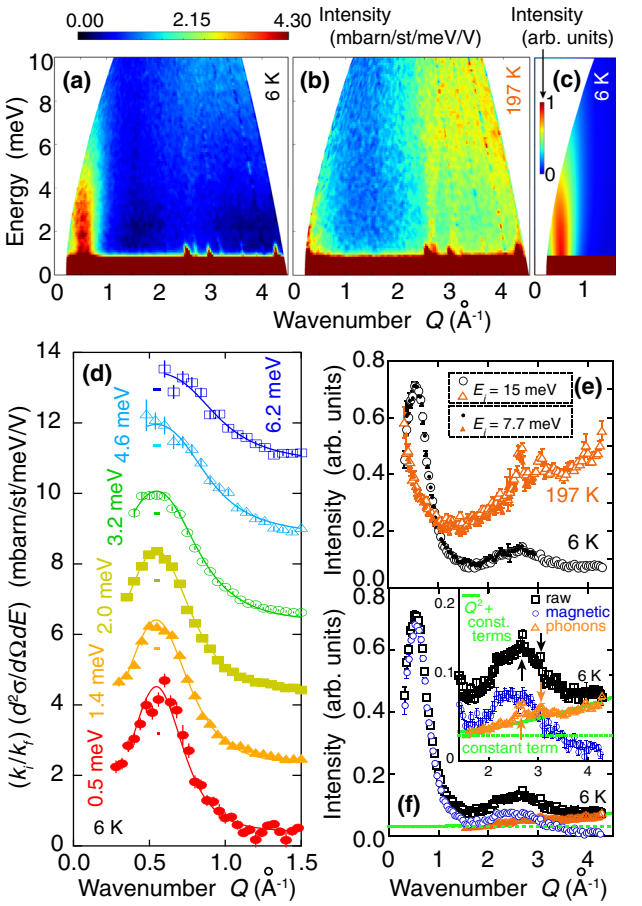

FIG. 1 (color online). (a)–(c) Experimental (a),(b) and calculated (c) contour plots of the scattering intensity distribution in (Q, E) space with $E_i = 15$ meV. (d) Constant-E cross sections in the low-Q range (symbols). From the bottom, $E_i = 3.1$, 15, 15, 15, 24, and 24 meV. The averaged E range was ±0.1, ±0.3, ±0.3, ±0.3, ±0.8, and ±0.8 meV. The vertical zero points are shifted by 2 mbarn st^{-1} meV^{-1} V^{-1}. The solid curves are fits of Eq. (2) to the data (see text). The tiny horizontal bars represent the Q resolution, which can be neglected compared to the experimental line widths. (e) Constant-E cross sections averaged in the 2.5 ± 0.5-meV range in (a) and (b). Those measured with $E_i = 7.7$ meV are also shown. (f) Extraction of the magnetic component. The inset magnifies the area of 2.4 Å^{-1} broad peak. The green lines indicate the phonon components described by Q^2 and constant terms and the arrows indicate the sharp peak phonon components.

We compare the E dependence of the 2.4-Å^{-1} magnetic peak and phonons, obtained in this way, and the 0.6-Å^{-1} magnetic peak in Fig. 2(g). The two magnetic E spectra are well homothetic to each other and exhibit the maximum around 2.5 meV. On the other hand, as E increases, the phonon intensity linearly increases and surpasses the magnetic intensity around 3 meV. Thus, to maximize

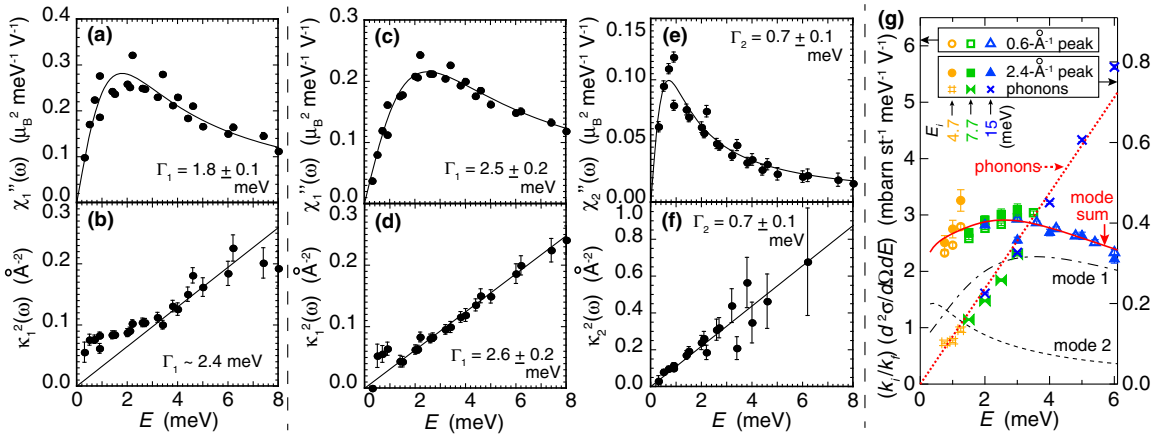

FIG. 2 (color online). Fitting results in the $n = 1$ (a),(b) and $n = 2$ models (c)–(g). Parts (a),(c),(e) show the $E = \hbar\omega$ dependence of the dynamic susceptibilities at Q_0, $\chi_j''(\omega)$; parts (b),(d),(f) show that of the Q-width parameters, $\kappa_j^2(\omega)$; (g) shows the E dependence of cross sections. In (g), the 0.6-Å^{-1} peak shows the 6-K raw data. The 2.4 Å^{-1} peak and phonons show the 6-K extracted magnetic and subtracted phonon components, respectively, as performed in Fig. 1(f). The averaged Q ranges were 0.55–0.95 Å^{-1} for all E_i for the 0.6-Å^{-1} peak, 2.0–2.3 Å^{-1} ($E_i = 4.7$ meV), 1.6–2.8 Å^{-1} ($E_i = 7.7$ meV), and 1.6–3.2 Å^{-1} ($E_i = 15$ meV) for the 2.4-Å^{-1} peak and phonons. The dotted straight line is a guide to the eye for the phonon data. In all the figure parts, the other lines are fits of Eqs. (3) and (4) to the data (see text).

the magnetic intensity, minimize the phonon intensity, and avoid the elastic tail, the aforementioned value of 2.5 meV was used as the representative E.

Analyses.—We analyze the fountainlike E evolution around 0.55 Å^{-1} at 6 K. The differential cross section of INS is proportional to the Bose factor $[1 - \exp(-\hbar\omega/k_BT)]^{-1}$ and the imaginary part $\chi''(Q,\omega)$ of the generalized magnetic susceptibility $\chi(Q,\omega)$, where $E = \hbar\omega$ [20]. Following a standard way to describe the spin fluctuations in nearly AF metals such as $Cr_{0.95}V_{0.05}$ and $La_{2-x}Sr_xCuO_4$ [21,22], we use

$$\chi(Q,\omega) = \sum_{j=1}^{n} \chi_j \left[1 + \frac{(Q-Q_0)^2}{\kappa_0^2} - i\frac{\omega}{\Gamma_j}\right]^{-1}, \quad (1)$$

where n is the number of spin fluctuation modes. This function corresponds to the expansion of the Lindhard function near the Fermi energy to describe a Fermi liquid [21–24]. The imaginary part of Eq. (1) is described by the following useful form [21]:

$$\chi''(Q,\omega) = \sum_{j=1}^{n} \chi_j''(\omega) \frac{\kappa_0^4 + \kappa_j^4(\omega)}{\{\kappa_0^2 + (Q-Q_0)^2\}^2 + \kappa_j^4(\omega)}, \quad (2)$$

where the ω evolutions are separated into the susceptibility at Q_0

$$\chi_j''(\omega) = \chi_j \frac{\omega\Gamma_j}{\omega^2 + \Gamma_j^2}, \quad (3)$$

and the Q width around Q_0

$$\kappa_j^2(\omega) = \kappa_0^2 \frac{\omega}{\Gamma_j}. \quad (4)$$

If Eq. (1) describes the data, an identical Γ_j will be obtained for both the susceptibility and the Q-width parts.

Figures 2(a) and 2(b) show the fitting results for an $n = 1$ model. The results coincide with the INS report of Lee *et al.* for both $\chi_1''(\omega)$ and Γ_1 [Fig. 2(a)] [7]. However, $\kappa_1^2(\omega)$ is not proportional to E in the low-E region [Fig. 2(b)]. This is rather consistent with the INS report of Murani *et al.* and the μSR data, suggesting the coexistence of another slower component below 1 meV [9,14]. Thus, we used an $n = 2$ model, and the fitting results are shown in Figs. 2(c)–2(f). $\chi_1''(\omega)$, $\kappa_1^2(\omega)$, $\chi_2''(\omega)$, and $\kappa_2^2(\omega)$ all fit well with $\Gamma_1 = 2.6$ meV and $\Gamma_2 = 0.7$ meV, where $\chi_1 = 0.43\,\mu_B^2\,\text{meV}^{-1}\,\text{V}^{-1}$, $\chi_2 = 0.20\,\mu_B^2\,\text{meV}^{-1}\,\text{V}^{-1}$, $Q_0 = 0.55$ Å^{-1}, and $\kappa_0 = 0.28$ Å^{-1}. Further, the E and $Q - E$ dependence of cross sections calculated from these parameters are shown in Fig. 2(g) (lines) and Fig. 1(c), respectively. Both are in good agreement with the experimental ones, as shown in Fig. 2(g) (symbols) and Fig. 1(a), respectively [25].

These Γ values coincide with those of Murani *et al.* within the errors, $\Gamma_1 = 1.5 \pm 0.5$ meV and $\Gamma_2 = 0.6 \pm 0.4$ meV at Q_0 at 6 K [14]. In addition, we would like to emphasize that our study presents the experimental and analysis results of Q widths [Figs. 1(d), 2(d), and 2(f); Eq. (4)] and those of overall $Q - E$ evolution [Figs. 1(a) and 1(c); Eqs. (2)–(4)] for the first time.

Next, we analyze the spatial correlations of the fluctuations from the obtained Q information. First, the value of Q_0 is equal to $0.72(2\pi/a) = 2\pi/\sqrt{2}a$, indicating the periodicity of $\sqrt{2}a = 4d_{V-V}$, where a denotes the lattice constant of 8.24 Å in the pyrochlore lattice [4], and d_{V-V} denotes the distance between the nearest-neighbor V sites, as shown in Fig. 3(a). This strongly suggests that the fluctuations consist of AF bonds of four V atoms along

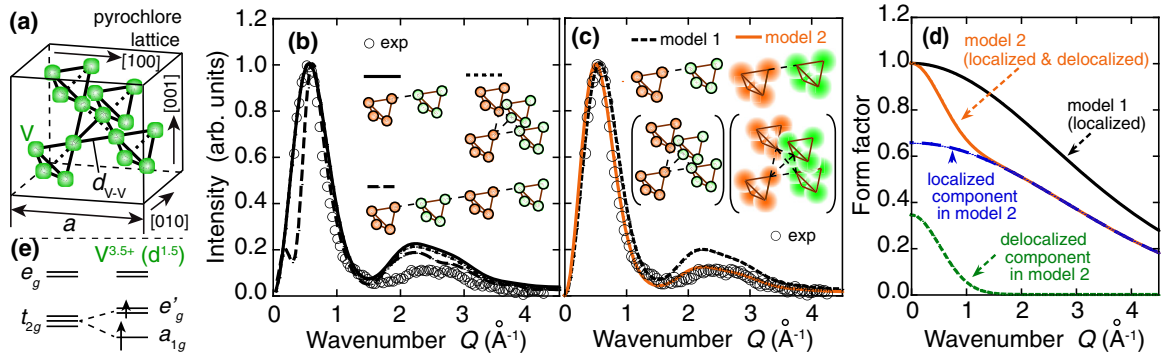

FIG. 3 (color online). Modeling of the dynamical spatial correlations. (a) Unit cell of the pyrochlore lattice. (b), (c) Comparisons of the experimental and model-calculated Q dependencies of the intensities. All intensities are normalized at the maximum intensity Q. The experimental data (open circles) are identical to the magnetic scattering in Fig. 1(f). The curves were calculated in the inset models, where the orange and green spheres denote the dynamically fluctuating up and down spins, respectively. In (c), the curves are drawn for the inset ditetrahedron models. The inset tetrahedrally arranged four-tetrahedron models with brackets also give nearly the same results within the line thickness. In (b) and (c), localized [model 1 in (d)] and modified [model 2 in (d)] magnetic form factors were used, respectively. (d) Magnetic form factors normalized at 0 Å^{-1}. The broken and dotted curves resolve the model-2 form factor into localized and delocalized components, respectively. (e) Energy scheme of the V orbitals. The arrows depict the Hund-rule filling of 1.5 electrons/V.

the $\langle 110 \rangle$ direction. Second, the value of the Q width κ_0 means ~5 Å of short correlation length. Third, as shown in Fig. 1(f), the Q dependence of the intensity consists of a combination of a strong broad 0.6-Å^{-1} peak and a weak broad 2.4-Å^{-1} peak. This combination is identical to that of the 4-meV mode observed in another highly frustrated spinel-type insulator, $GeCo_2O_4$ [30], which is explained by AF ditetrahedron spin correlations by single-crystal INS [31]. Furthermore, this ditetrahedron structure satisfies the first and second conditions. Thus, the fluctuations are most likely based on the ditetrahedron in the spatial correlations.

We calculated the Q dependence of the intensities for several ditetrahedron-based models, and three of these models are shown in Fig. 3(b), where a localized theoretical magnetic form factor was used [32]. As expected, every model roughly reproduces the 0.6 and 2.4-Å^{-1} positions, and the ditetrahedron model and the tetrahedrally arranged-four-tetrahedron model, of which the Q-dependence curves are nearly the same as each other, are also consistent with the experimental data for the 0.6-Å^{-1} peak width.

However, the calculated intensities of the 2.4-Å^{-1} peak are much stronger than the experimental data. To improve this, we incorporated the spatial expansion of the spin density distribution at each V site, considering that LiV_2O_4 exhibits metallic electrical resistivity. This itinerancy suggests the rapid decrease in the magnetic form factor in Q space. Further, band calculations indicate that the Fermi level is mainly crossed by V 3d t_{2g} orbital bands, which roughly split into a localized a_{1g} singlet and a delocalized e'_g doublet via a small trigonal crystal field, as schematically shown in Fig. 3(e) [33,34]. Thus, for simplicity, we approximated the magnetic form factor by $\alpha f_{\text{localized}}(Q) + (1-\alpha)\exp(-Q^2/\Delta Q_{\text{delocalized}})$, where $f_{\text{localized}}(Q)$ denotes the localized form factor [32] normalized at 0 Å^{-1}, and α and $\Delta Q_{\text{delocalized}}$ are determined to fit the experimental data.

Figure 3(c) shows a comparison among the experimental data, localized model 1, and model 2 with localization and delocalization. The experimental data are well fit to model 2, which is much better than model 1 with respect to the 2.4 Å^{-1} intensity and the 0.6-Å^{-1} peak profile. The model-2 fitting was obtained at $\alpha = 0.66$ and $\Delta Q_{\text{delocalized}} = 0.74$ Å^{-1}. The value of α indicates $\alpha : (1-\alpha) = 1.0 : 0.5$, which is in excellent agreement with the Hund-rule filling of 1 a_{1g} and 0.5 e'_g electrons/V, as shown in Fig. 3(e). The $\Delta Q_{\text{delocalized}}$ value mean 2.2 Å of spatial distribution at half width at half maximum, which is much larger than $(d_{V-V}/2) = 1.5$ Å. This indicates that the delocalized components of the nearest-neighbor V spins considerably overlap with each other in the polytetrahedron.

Discussion.—The observed dynamical magnetic susceptibility is well described by a simple function for a Fermi liquid [Eq. (1)] and is accompanied with the delocalization in the magnetic form factor. These facts verify the treatments of spin fluctuations in itinerant systems, such as a series of self-consistent renormalization theories, demonstrating that the spin-fluctuation channel dominates HF formation [10,35,36]. The partially delocalized magnetic form factor, which is highly characteristic in 3d systems, is discussed in the Supplemental Material [25].

The spin fluctuations are based on the AF polytetrahedron in the spatial correlations. This strongly suggests that geometrical frustration causes the fluctuations as well as in $GeCo_2O_4$ [31], and that the large HF entropy originates from the high degeneracy driven by frustration.

Interestingly, the polytetrahedron combines both theoretically proposed characteristics, the 1D-like chains along the $\langle 110 \rangle$ directions and the ferromagnetic tetrahedron

units, which are accompanied by spin-orbit fluctuations [15,16]. In the former theory [16], 1D correlations occur to release geometrical frustration, taking into account the fact that a pyrochlore lattice consists of 1D chains along the $\langle 110 \rangle$ directions, as shown in Fig. 3(a). The V t_{2g} orbitals hybridize with each other to form the 1D Hubbard chains with a periodicity of $4d_{V-V}$. In the latter theory [15], the ferromagnetic tetrahedra form to release frustration because a pyrochlore lattice is also regarded as the tetrahedra arranged in a face-centered-cubic lattice. The molecular orbital formation of the V_4 tetramer remarkably decreases the system energy.

Summary.—We studied spin fluctuations over a wide (Q, E) space in LiV_2O_4 by INS. The observed data can be described by a simple response function, a partially delocalized magnetic form factor, and AF polytetrahedron-based spatial correlations. With these characteristics, the large HF entropy is attributable to frustration with spin-orbit fluctuations and remarkable orbital hybridization. Our study will promote future studies of novel quasiparticles as a prototype in the long-standing many-body problem.

We thank Dr. S. Iikubo for assisting with the sample preparation and Dr. M. Yokoyama for providing the preliminary neutron machine time. The neutron experiments were performed with the approval of Japan Proton Accelerator Research Complex (J-PARC) (2012A0146 and partially 2012P0202). This study was financially supported by Grants-in-Aid for Young Scientists (B) (22740209 and 26800174) and Priority Areas (22014001) from the MEXT of Japan.

*tomiyasu@m.tohoku.ac.jp

[1] L. D. Landau and E. M. Lifshitz, *Statistical Physics, Part 2*, Course of Theoretical Physics Vol. 9 (Pergamon, Oxford, 1981).
[2] S. Kondo *et al.*, Phys. Rev. Lett. **78**, 3729 (1997).
[3] C. Urano, M. Nohara, S. Kondo, F. Sakai, H. Takagi, T. Shiraki, and T. Okubo, Phys. Rev. Lett. **85**, 1052 (2000).
[4] Y. Matsushita, H. Ueda, and Y. Ueda, Nature (London) **4**, 845 (2005).
[5] S. Das, X. Zong, A. Niazi, A. Ellern, J. Q. Yan, and D. C. Johnston, Phys. Rev. B **76**, 054418 (2007).
[6] H. Wada, H. Nakamura, E. Fukami, K. Yoshimura, M. Shiga, and Y. Nakamura, J. Magn. Magn. Mater. **70**, 17 (1987).
[7] S.-H. Lee, Y. Qiu, C. Broholm, Y. Ueda, and J. J. Rush, Phys. Rev. Lett. **86**, 5554 (2001).
[8] Y. Shimizu, H. Takeda, M. Tanaka, M. Itoh, S. Niitaka, and H. Takagi, Nat. Commun. **3**, 981 (2012).
[9] R. Kadono, A. Koda, W. Higemoto, K. Ohishi, H. Ueda, C. Urano, S. Kondo, M. Nohara, and H. Takagi, J. Phys. Soc. Jpn. **81**, 014709 (2012).
[10] V. Yushankhai, A. Yaresko, P. Fulde, and P. Thalmeier, Phys. Rev. B **76**, 085111 (2007).
[11] P. E. Jönsson, K. Takenaka, S. Niitaka, T. Sasagawa, S. Sugai, and H. Takagi, Phys. Rev. Lett. **99**, 167402 (2007).
[12] A. Shimoyamada *et al.*, Phys. Rev. Lett. **96**, 026403 (2006).
[13] R. Arita, K. Held, A. V. Lukoyanov, and V. I. Anisimov, Phys. Rev. Lett. **98**, 166402 (2007).
[14] A. P. Murani, A. Krimmel, J. R. Stewart, M. Smith, P. Strobel, A. Loidl, and A. Ibarra-Palos, J. Phys. Condens. Matter **16**, S607 (2004).
[15] K. Hattori and H. Tsunetsugu, Phys. Rev. B **79**, 035115 (2009).
[16] S. Fujimoto, Phys. Rev. B **65**, 155108 (2002).
[17] K. Nakajima *et al.*, J. Phys. Soc. Jpn. **80**, SB028 (2011).
[18] Y. Inamura, T. Nakatani, J. Suzuki, and T. Otomo, J. Phys. Soc. Jpn. **82**, SA031 (2013).
[19] S. Kondo, D. C. Johnston, and L. L. Miller, Phys. Rev. B **59**, 2609 (1999).
[20] S. W. Lovesey, *Theory of Neutron Scattering from Condensed Matter* (Oxford University Press, New York, 1984).
[21] S. M. Hayden, R. Doubble, G. Aeppli, T. G. Perring, and E. Fawcett, Phys. Rev. Lett. **84**, 999 (2000).
[22] Y. Zha, V. Barzykin, and D. Pines, Phys. Rev. B **54**, 7561 (1996).
[23] T. Moriya, Phys. Rev. Lett. **24**, 1433 (1970).
[24] T. Moriya and K. Ueda, Adv. Phys. **49**, 555 (2000).
[25] See Supplemental Material at http://link.aps.org/supplemental/10.1103/PhysRevLett.113.236402 for details of analysis results, which includes Refs. [26–29].
[26] P. D. DeCicco and A. Kitz, Phys. Rev. **162**, 486 (1967).
[27] A. Alatas, A. H. Said, H. Sinn, G. Bortel, M. Y. Hu, J. Zhao, C. A. Burns, E. Burkel, and E. E. Alp, Phys. Rev. B **77**, 064301 (2008).
[28] A. Zheludev, V. Barone, M. Bonnet, B. Delley, A. Grand, E. Ressouche, P. Rey, R. Subra, and J. Schweizer, J. Am. Chem. Soc. **116**, 2019 (1994).
[29] A. Zheludev, A. Grand, E. Ressouche, J. Scbweizer, J. Brian, C. Morin, A. J. Epstein, D. A. Dixon, and J. S. Miller, J. Am. Chem. Soc. **116**, 7243 (1994).
[30] J. C. Lashley, R. Stevens, M. K. Crawford, J. Boerio-Goates, B. F. Woodfield, Y. Qiu, J. W. Lynn, P. A. Goddard, and R. A. Fisher, Phys. Rev. B **78**, 104406 (2008).
[31] K. Tomiyasu *et al.*, Phys. Rev. B **84**, 054405 (2011).
[32] M. Iwata, Acta Crystallogr. Sect. B **33**, 59 (1977).
[33] J. Matsuno, A. Fujimori, and L. F. Mattheiss, Phys. Rev. B **60**, 1607 (1999).
[34] V. I. Anisimov, M. A. Korotin, M. Zölfl, T. Pruschke, K. LeHur, and T. M. Rice, Phys. Rev. Lett. **83**, 364 (1999).
[35] V. Yushankhai, P. Thalmeier, and T. Takimoto, Phys. Rev. B **77**, 125126 (2008).
[36] V. Yushankhai, T. Takimoto, and P. Thalmeier, Phys. Rev. B **82**, 085112 (2010).